T.N. Mishra* and K.N. Rai

Highly Accurate Compact Difference Scheme for SPL Heat Conduction Model of General Body

DOI 10.1515/zna-2016-0067
Received February 21, 2016; accepted August 25, 2016; previously published online October 10, 2016

Abstract: Heat transport based on SPL model is of vital importance in microtechnological applications. The heat transport equation is different from the traditional heat conduction equation due to the presence of lagging parameter. In this article, the heat transport in the general body based on SPL heat conduction model under Neumann (insulated) boundary condition is solved by high-order compact difference scheme. The solution is obtained by extending the idea of Dai for discretising Neumann (insulated) boundary condition of heat conduction to the SPL heat conduction model and avoid the need of discretising Neumann boundary conditions. The stability of the numerical scheme has been discussed and observed that the present scheme is unconditionally stable. Model is validated for the thin film of silicon and found that SPL model give the satisfactory results in the macro- and microtemporal scales and up to microspatial scale. A numerical example of particular interest has been studied and discussed in details.

Keywords: Finite Difference Scheme; Neumann Boundary Condition; Silicon Film; SPL Heat Conduction Model; Unconditional Stability.

1 Introduction

Cattaneo [1] and Vernotte [2] removed the deficiency [3–5] occurs in the classical heat conduction equation based on Fourier law by adding a lagging term in Fourier law and proposed the CV constitutive relation in the form of

$$\tau\frac{\partial \mathbf{q}^*}{\partial t^*}+\mathbf{q}^*=-k\nabla T, \tag{1}$$

where k is the thermal conductivity of medium and τ the material property called the lagging time. This model characterises the combined diffusion and wave like behavior of heat conduction and predicts a finite speed

$$c=\left(\frac{k}{\rho c_b \tau}\right)^{1/2} \tag{2}$$

for heat propagation [6], where ρ is the density and c_b the specific heat capacity. For more details about thermal lagging in wave theory, see [7, 8]. Tzou [9–13] generalised the CV heat conduction model (1) as

$$\mathbf{q}^*(\mathbf{r}, t^*+\tau)=-k\nabla T(\mathbf{r}, t^*), \tag{3}$$

The above equation (3) is known as single-phase-lagging (SPL) heat conduction model. This model establishes the heat flux (the result) when a temperature gradient (the cause) is suddenly imposed.

Due to the complexity of the SPL heat conduction model, the exact temperature solutions can only be obtained for the particular initial and boundary conditions. However, problem involving Neumann boundary condition [14–18], the discretisation of boundary conditions must dealt carefully to match global accuracy, as it involves discresation error. The first-order accurate or second-order accurate finite difference discretisation for the Neumann boundary condition needs to discretise points outside to the boundary [19, 20]. Dai [21] observed that the accuracy of the numerical scheme is affected when the first-order accurate finite difference scheme for the Neumann boundary condition is employed and a second-order numerical scheme is employed at the interior grid points. Further, it was found that stability of overall numerical scheme is also affected when a second-order accurate finite difference scheme [20] is employed for discretising Neumann boundary condition.

In the present investigation, we have utilised the idea of Dai [21] for discretising Neumann boundary condition of heat conduction, to the SPL heat conduction model of general body (i.e. plate, cylinder and sphere), and avoid the need of ghost point outside the boundary. Model is validated by taking particular example of thin film of silicon and the effect of different parameters on temperature solution will be investigated.

The effect of spatial and temporal grid size on stability of numerical scheme has also been investigated

***Corresponding author: T.N. Mishra,** DST-CIMS, Faculty of Science, BHU, Varanasi, Uttar Pradesh, India, Tel.: +919198006395, E-mail: t.mishra01@gmail.com
K.N. Rai: Mathematical Sciences, IIT BHU, Varanasi, Uttar Pradesh, India

and found that stability is independent of grid size. The outline of the remainder of this article is as follows. In Section 2, SPL heat conduction equation is presented. Solution of the SPL heat conduction model is given in Section 3. Section 4 presents the stability of the numerical scheme. Model validation is given in Section 5. Section 6 contains numerical examples. Concluding remarks are summarised in Section 7.

2 SPL Heat Conduction Model

The combination of Fourier law of heat conduction

$$\mathbf{q}^* = -k\frac{\partial T}{\partial y} \tag{4}$$

and law of conservation of energy

$$\rho c_b \frac{\partial T}{\partial t^*} = -\frac{\partial \mathbf{q}^*}{\partial y} + g^* \tag{5}$$

provides the law of heat conduction as follows,

$$\rho c_b \frac{\partial T}{\partial t^*} = k\frac{\partial^2 T}{\partial y^2} + g^* \tag{6}$$

where g^* is the internal heat source. Equation (1) together with the energy conservation (5) gives the SPL heat conduction equation

$$\frac{\partial T}{\partial t^*} + \tau\frac{\partial^2 T}{\partial t^{*2}} = \alpha\frac{\partial^2 T}{\partial y^2} + \frac{\alpha}{k}\left(g^* + \tau\frac{\partial g^*}{\partial t^*}\right) \tag{7}$$

where α is the thermal diffusivity of the material and the lagging time $\tau = \alpha/c^2$. If heat propagate with an infinite speed, i.e. $c \to \infty$ then $\tau = 0$ and hence above (7) becomes parabolic heat conduction equation based on Fourier law, (6). By introducing dimensionless parameters

$$\theta = \frac{kcT}{\alpha f_r},\ x = \frac{cy}{2\alpha},\ t = \frac{c^2 t^*}{2\alpha} \text{ and } g = \frac{4\alpha g*}{cf_r},$$

the (7) can be expressed in dimensionless form as

$$2\frac{\partial \theta}{\partial t} + \frac{\partial^2 \theta}{\partial t^2} = \frac{\partial^2 \theta}{\partial x^2} + g + \frac{1}{2}\frac{\partial g}{\partial t} \tag{8}$$

In the present investigation, a one-dimensional SPL model for general body

$$2\frac{\partial \theta}{\partial t} + \frac{\partial^2 \theta}{\partial t^2} = \frac{1}{R^\Gamma}\frac{\partial}{\partial R}\left(R^\Gamma \frac{\partial \theta}{\partial R}\right) + \left(g + \frac{1}{2}\frac{\partial g}{\partial t}\right) \tag{9}$$

has been considered. Assume that body, $(0 < R < l)$, has constant thermophysical properties and uniform thickness. Initially, the body is at temperature $\theta(R, 0) = f_1(R)$ and initial time rate of change in temperature is $f_2(R)$. For time $t > 0$, boundaries of body are insulated and either of the boundaries can be heated by internal laser heat source. The following initial and boundary conditions will be considered in this study

$$\theta(R,\ 0) = f_1(R),\quad \frac{\partial \theta(R,\ 0)}{\partial t} = f_2(R) \tag{10}$$

$$\frac{\partial \theta(0,\ t)}{\partial R} = 0,\quad \frac{\partial \theta(l,\ t)}{\partial R} = 0 \tag{11}$$

3 Solution

To establish the numerical approximation scheme, let $\Delta R = h = \frac{l}{N} > 0$ and $\Delta t = \frac{t}{M}$ be the grid size in space and time directions, respectively. The grid points in the space interval $[0, l]$ are the numbers $R_j = jh$, $j = 0, 1, 2, 3 \ldots N$ and grid points in the time interval $[0, t]$ are labelled $t_n = n\Delta t$, $n = 1, 2, \ldots, M$. The values of the functions θ at grid points are denoted by $\theta_j^n = \theta(R_j, t_n)$.

Case I. $\Gamma = 0$ *and* $R = x$*, i.e. body is a one-dimensional thin plate*.

In this Case for solving the (9)–(11), if we discretise (9) by using fourth-order implicit compact finite difference scheme [22–24]

$$\begin{aligned}
&2\left(\frac{\theta_{j-1}^{n+1} - \theta_{j-1}^n}{10\Delta t} + \frac{\theta_j^{n+1} - \theta_j^n}{\Delta t} + \frac{\theta_{j+1}^{n+1} - \theta_{j+1}^n}{10\Delta t}\right) \\
&+ \frac{\theta_{j-1}^{n+1} - 2\theta_{j-1}^n + \theta_{j-1}^{n-1}}{10(\Delta t)^2} + \frac{\theta_j^{n+1} - 2\theta_j^n + \theta_j^{n-1}}{(\Delta t)^2} + \frac{\theta_{j+1}^{n+1} - 2\theta_{j+1}^n + \theta_{j+1}^{n-1}}{10(\Delta t)^2} \\
&= \frac{6}{10h^2}(\theta_{j-1}^{n+1} - 2\theta_j^{n+1} + \theta_{j+1}^{n+1}) + \frac{6}{10h^2}(\theta_{j-1}^n - 2\theta_j^n + \theta_{j+1}^n) + g_j^{n+\frac{1}{2}}
\end{aligned} \tag{12}$$

at the interior points x_j, $2 \le j \le N-1$, then the values of θ_{xx} at the boundary points should be provided, which are usually inconvenient to obtain. To overcome this deficiency, Dai [21] employ a combined compact finite difference approximation at x_1 and x_N and discretised the boundary condition, (11), at x_1 and x_N as follows:

$$\begin{aligned}
a\theta_{xx}(x_1,\ t) + b\theta_{xx}(x_2,\ t) &\approx \frac{c}{h^2}[\theta(x_2,\ t) - \theta(x_1,\ t)] \\
&- \frac{1}{h}\theta_x(x_1 - \bar{\theta}_1 h,\ t)
\end{aligned} \tag{13}$$

$$b^*\theta_{xx}(x_{N-1},\,t)+a^*\theta_{xx}(x_N,\,t)\approx-\frac{c^*}{h^2}[\theta(x_N,\,t)-\theta(x_{N-1},\,t)]+\frac{1}{h}\theta_x(x_N+\bar{\theta}_2 h,\,t) \tag{14}$$

where $a=1=a^*$, $b=\frac{1}{2}+\frac{\sqrt{3}}{3}=b^*$ and N is the number of interior grid points. The grid size and the coordinates of the grid points are given as follows

$$h=\frac{L}{N+\bar{\theta}_1+\bar{\theta}_2-1},\quad x_j=(j-1+\bar{\theta}_1)h,\quad j=1,\,2\ldots,\,N. \tag{15}$$

where $\bar{\theta}_1 h$ and $\bar{\theta}_2 h$ are the distances of actual left boundary and x_1 and actual right boundary and x_N, respectively. Thus, the Neumann boundary condition is directly used in (13) and (14) without discretising. Hence, a high-order compact finite difference scheme for (11) at x_1 and x_N can be written as follows:

$$2a\frac{\theta_1^{n+1}-\theta_1^n}{\Delta t}+2b\frac{\theta_2^{n+1}-\theta_2^n}{\Delta t}+a\frac{\theta_1^{n+1}-2\theta_1^n+\theta_1^{n-1}}{(\Delta t)^2}+b\frac{\theta_2^{n+1}-2\theta_2^n+\theta_2^{n-1}}{(\Delta t)^2}=\frac{c}{h^2}\frac{\theta_2^{n+1}-\theta_1^{n+1}}{2}+\frac{c}{h^2}\frac{\theta_2^n-\theta_1^n}{2}+g_1^{n+\frac{1}{2}} \tag{16}$$

$$2b^*\frac{\theta_{N-1}^{n+1}-\theta_{N-1}^n}{\Delta t}+2a^*\frac{\theta_N^{n+1}-\theta_N^n}{\Delta t}+b^*\frac{\theta_{N-1}^{n+1}-2\theta_{N-1}^n+\theta_{N-1}^{n-1}}{(\Delta t)^2}+a^*\frac{\theta_N^{n+1}-2\theta_N^n+\theta_N^{n-1}}{(\Delta t)^2}=-\frac{c^*}{h^2}\frac{\theta_N^{n+1}-\theta_{N-1}^{n+1}}{2}-\frac{c^*}{h^2}\frac{\theta_N^n-\theta_{N-1}^n}{2}+g_1^{n+\frac{1}{2}} \tag{17}$$

Thus, a high-order compact finite difference scheme consists of (12) for interior grid points x_j, $j=2,\,\ldots\,N-1$, and (16)–(17) for two grid points x_1 and x_N. The truncation error at interior grid points $(x_j,\,t_{n+(1/2)})$, $j=2,\,\ldots,\,N$, of the scheme is of order $(\Delta t+h^4)$ and $(\Delta t+h^3)$ at grid points x_1 and x_N. Thus, from (12), (16), and (17), we get dimensionless temperature (θ).

Case II. $\Gamma=1$ *and* $R=r$, *i.e. body is a one-dimensional thin cylinder.*

To solve the (9)–(11), for the thin cylinder, we discretise (9) using fourth-order implicit compact finite difference scheme [22–24]

$$2\left(\frac{\theta_{j-1}^{n+1}-\theta_{j-1}^n}{10\Delta t}+\frac{\theta_j^{n+1}-\theta_j^n}{\Delta t}+\frac{\theta_{j+1}^{n+1}-\theta_{j+1}^n}{10\Delta t}\right)+\frac{\theta_{j-1}^{n+1}-2\theta_{j-1}^n+\theta_{j-1}^{n-1}}{10(\Delta t)^2}+\frac{\theta_j^{n+1}-2\theta_j^n+\theta_j^{n-1}}{(\Delta t)^2}+\frac{\theta_{j+1}^{n+1}-2\theta_{j+1}^n+\theta_{j+1}^{n-1}}{10(\Delta t)^2}=\frac{6}{10h^2 r_j}\left\{r_{j+\frac{1}{2}}(\theta_{j+1}^{n+1}-\theta_j^{n+1})-r_{j-\frac{1}{2}}(\theta_j^{n+1}-\theta_{j-1}^{n+1})\right\}+\frac{6}{10h^2 r_j}\left\{r_{j+\frac{1}{2}}(\theta_{j+1}^{n}-\theta_j^{n})-r_{j-\frac{1}{2}}(\theta_j^{n}-\theta_{j-1}^{n})\right\} \tag{18}$$

Now we may employ combined compact difference approximation at r_1, which is point next to the left boundary, as follows:

$$a\frac{\partial}{\partial r}\left(r\frac{\partial\theta(r,\,t)}{\partial r}\right)_1+b\frac{\partial}{\partial r}\left(r\frac{\partial\theta(r,\,t)}{\partial r}\right)_2=\frac{c}{h^2}r_{\frac{3}{2}}[\theta(r_2,\,t)-\theta(r_1,\,t)]-\frac{r_1}{h}\frac{\partial\theta(r_1-\bar{\theta}_1 h,\,t)}{\partial r} \tag{19}$$

where a, b, c, and $\bar{\theta}_1$ are constants to be determined and $\bar{\theta}_1\geq 0$. Now expanding each term of (19) by Taylor series at r_1 and matching the coefficients of both sides, we get

$$a+b=\frac{1}{h}\left(cr_{\frac{3}{2}}-r_1\right) \tag{20}$$

$$2(ar_1+bh+br_2)=\left(cr_{\frac{3}{2}}+2r_1\bar{\theta}_1\right) \tag{21}$$

$$3bh+6br_2=\left(cr_{\frac{3}{2}}-3r_1\bar{\theta}_1^2\right) \tag{22}$$

$$4bh+12br_2=\left(cr_{\frac{3}{2}}+4r_1\bar{\theta}_1^3\right) \tag{23}$$

Thus, by dropping the truncation error $O(h^3)$, a third-order combined compact difference scheme at r_1 is obtained as follows:

$$a\frac{\partial}{\partial r}\left(r\frac{\partial\theta(r,\,t)}{\partial r}\right)_1+b\frac{\partial}{\partial r}\left(r\frac{\partial\theta(r,\,t)}{\partial r}\right)_2\approx\frac{c}{h^2}r_{\frac{3}{2}}[\theta(r_2,\,t)-\theta(r_1,\,t)]-\frac{r_1}{h}\frac{\partial\theta(r_1-\bar{\theta}_1 h,\,t)}{\partial r} \tag{24}$$

where the constants a, b, c, and $\bar{\theta}_1$ are obtained from (20)–(23).

Similarly, combined compact difference approximation at r_N, which is point next to the right boundary can be obtained as follows:

$$b^*\frac{\partial}{\partial r}\left(r\frac{\partial\theta(r,\,t)}{\partial r}\right)_{N-1}+a^*\frac{\partial}{\partial r}\left(r\frac{\partial\theta(r,\,t)}{\partial r}\right)_N\approx -\frac{c^*}{h^2}r_{N-\frac{1}{2}}[\theta(r_N,\,t)-\theta(r_{N-1},\,t)]+\frac{r_N}{h}\frac{\partial\theta(r_N+\bar{\theta}_2h,\,t)}{\partial r} \tag{25}$$

where N is the number of interior grid points. The grid size and the coordinates of the grid points are given as follows:

$$h=\frac{L}{N+\bar{\theta}_1+\bar{\theta}_2-1},\quad r_j=(j-1+\bar{\theta}_1)h,\quad j=1,\,2\ldots,\,N. \tag{26}$$

where $\bar{\theta}_1h$ and $\bar{\theta}_2h$ are the distances of actual left boundary and r_1 and actual right boundary and r_N, respectively. Thus, the Neumann boundary condition is directly used in (24) and (25) without discretising. Hence, a high-order compact difference scheme for (11) at r_1 and r_N can be written as follows:

$$2a\frac{\theta_1^{n+1}-\theta_1^n}{\Delta t}+2b\frac{\theta_2^{n+1}-\theta_2^n}{\Delta t}+a\frac{\theta_1^{n+1}-2\theta_1^n+\theta_1^{n-1}}{(\Delta t)^2}+b\frac{\theta_2^{n+1}-2\theta_2^n+\theta_2^{n-1}}{(\Delta t)^2}=\frac{c}{r_1}r_{\frac{3}{2}}\frac{\theta_2^{n+1}-\theta_1^{n+1}}{2h^2}+\frac{c}{r_1}r_{\frac{3}{2}}\frac{\theta_2^n-\theta_1^n}{2h^2}+g_1^{n+\frac{1}{2}} \tag{27}$$

$$2b^*\frac{\theta_{N-1}^{n+1}-\theta_{N-1}^n}{\Delta t}+2a^*\frac{\theta_N^{n+1}-\theta_N^n}{\Delta t}+b^*\frac{\theta_{N-1}^{n+1}-2\theta_{N-1}^n+\theta_{N-1}^{n-1}}{(\Delta t)^2}+a^*\times\frac{\theta_N^{n+1}-2\theta_N^n+\theta_N^{n-1}}{(\Delta t)^2}=-\frac{c^*}{r_N}r_{N-\frac{1}{2}}\frac{\theta_N^{n+1}-\theta_{N-1}^{n+1}}{2h^2}-\frac{c^*}{r_N}r_{N-\frac{1}{2}}\frac{\theta_N^n-\theta_{N-1}^n}{2h^2}+g_N^{n+\frac{1}{2}} \tag{28}$$

Thus, a high-order compact finite difference scheme consists of (18) for interior grid points r_j, $j=2,\ldots N-1$, and (27)–(28) for two grid points r_1 and r_N. The truncation error at interior grid points $(r_j,\,t_{n+(1/2)})$, $j=2,\ldots,N$, of the scheme is of order $(\Delta t+h^4)$ and $(\Delta t+h^3)$ at grid points r_1 and r_N. Thus, from (18), (27), and (28), we get dimensionless temperature (θ).

Case III. $\Gamma=2$ *and* $R=r$, *i.e. body is a one-dimensional thin sphere.*

In *Case* of sphere, we discretise (9) by using fourth-order implicit compact finite difference scheme [22–24]

$$2\left(\frac{\theta_{j-1}^{n+1}-\theta_{j-1}^n}{10\Delta t}+\frac{\theta_j^{n+1}-\theta_j^n}{\Delta t}+\frac{\theta_{j+1}^{n+1}-\theta_{j+1}^n}{10\Delta t}\right)+\frac{\theta_{j-1}^{n+1}-2\theta_{j-1}^n+\theta_{j-1}^{n-1}}{10(\Delta t)^2}+\frac{\theta_j^{n+1}-2\theta_j^n+\theta_j^{n-1}}{(\Delta t)^2}+\frac{\theta_{j+1}^{n+1}-2\theta_{j+1}^n+\theta_{j+1}^{n-1}}{10(\Delta t)^2}=\frac{6}{10h^2r_j^2}\left\{r^2_{j+\frac{1}{2}}(\theta_{j+1}^{n+1}-\theta_j^{n+1})-r^2_{j-\frac{1}{2}}(\theta_j^{n+1}-\theta_{j-1}^{n+1})\right\}+\frac{6}{10h^2r_j^2}\left\{r^2_{j+\frac{1}{2}}(\theta_{j+1}^{n}-\theta_j^{n})-r^2_{j-\frac{1}{2}}(\theta_j^{n}-\theta_{j-1}^{n})\right\} \tag{29}$$

Now we may employ combined compact difference approximation at r_1, which is point next to the left boundary, as follows:

$$a\frac{\partial}{\partial r}\left(r^2\frac{\partial\theta(r,\,t)}{\partial r}\right)_1+b\frac{\partial}{\partial r}\left(r^2\frac{\partial\theta(r,\,t)}{\partial r}\right)_2=\frac{c}{h^2}r^2_{\frac{3}{2}}[\theta(r_2,\,t)-\theta(r_1,\,t)]-\frac{r_1^2}{h}\frac{\partial\theta(r_1-\bar{\theta}_1h,\,t)}{\partial r} \tag{30}$$

where a, b, c, and $\bar{\theta}_1$ are constants to be determined and $\bar{\theta}_1\geq 0$. Now expanding each term of (30) by Taylor series at r_1 and matching the coefficients of both sides we get

$$2(a+b)=\frac{1}{h}\left(cr^2_{\frac{3}{2}}-r_1^2\right) \tag{31}$$

$$2(ar_1^2+2bhr_2+br_2^2)=\left(cr^2_{\frac{3}{2}}+2r_1^2\bar{\theta}_1\right) \tag{32}$$

$$6(br_2h+6br_2^2)=\left(cr^2_{\frac{3}{2}}-3r_1^2\bar{\theta}_1^2\right) \tag{33}$$

$$4br_2h+12br_2^2=\left(cr^2_{\frac{3}{2}}+4r_1^2\bar{\theta}_1^3\right) \tag{34}$$

Thus, by dropping the truncation error $O(h^3)$, a third-order combined compact difference scheme at r_1 is obtained as follows:

$$a\frac{\partial}{\partial r}\left(r^2\frac{\partial\theta(r,\,t)}{\partial r}\right)_1+b\frac{\partial}{\partial r}\left(r^2\frac{\partial\theta(r,\,t)}{\partial r}\right)_2\approx\frac{c}{h^2}r^2_{\frac{3}{2}}[\theta(r_2,\,t)-\theta(r_1,\,t)]-\frac{r_1^2}{h}\frac{\partial\theta(r_1-\bar{\theta}_1h,\,t)}{\partial r} \tag{35}$$

where the constants a, b, c, and $\bar{\theta}_1$ are obtained from (31)–(34).

Similarly, combined compact difference approximation at r_N, which is point next to the right boundary, can be obtained as follows:

$$b^*\frac{\partial}{\partial r}\left(r^2\frac{\partial\theta(r,t)}{\partial r}\right)_{N-1}+a^*\frac{\partial}{\partial r}\left(r^2\frac{\partial\theta(r,t)}{\partial r}\right)_N$$
$$\approx-\frac{c^*}{h^2}r^2_{N-\frac{1}{2}}[\theta(r_N,t)-\theta(r_{N-1},t)]+\frac{r_N^2}{h}\frac{\partial\theta(r_N+\bar{\theta}_2h,t)}{\partial r} \quad (36)$$

where N is the number of interior grid points. The grid size and the coordinates of the grid points are given as follows:

$$h=\frac{L}{N+\bar{\theta}_1+\bar{\theta}_2-1},\quad r_j=(j-1+\bar{\theta}_1)h,\quad j=1,2\ldots,N. \quad (37)$$

where $\bar{\theta}_1h$ and $\bar{\theta}_2h$ are the distances of actual left boundary and r_1 and actual right boundary and r_N, respectively. Thus, the Neumann boundary condition is directly used in (35) and (36) without discretising. Hence, the compact difference scheme for (11) at r_1 and r_N can be written as follows:

$$2a\frac{\theta_1^{n+1}-\theta_1^n}{\Delta t}+2b\frac{\theta_2^{n+1}-\theta_2^n}{\Delta t}+a\frac{\theta_1^{n+1}-2\theta_1^n+\theta_1^{n-1}}{(\Delta t)^2}$$
$$+b\frac{\theta_2^{n+1}-2\theta_2^n+\theta_2^{n-1}}{(\Delta t)^2}=\frac{c}{r_1^2}r^2_{\frac{3}{2}}\frac{\theta_2^{n+1}-\theta_1^{n+1}}{2h^2}+\frac{c}{r_1^2}r^2_{\frac{3}{2}}\frac{\theta_2^n-\theta_1^n}{2h^2}+g_1^{n+\frac{1}{2}} \quad (38)$$

$$2b^*\frac{\theta_{N-1}^{n+1}-\theta_{N-1}^n}{\Delta t}+2a^*\frac{\theta_N^{n+1}-\theta_N^n}{\Delta t}+b^*\frac{\theta_{N-1}^{n+1}-2\theta_{N-1}^n+\theta_{N-1}^{n-1}}{(\Delta t)^2}$$
$$+a^*\frac{\theta_N^{n+1}-2\theta_N^n+\theta_N^{n-1}}{(\Delta t)^2}=-\frac{c^*}{r_N^2}r^2_{N-\frac{1}{2}}\frac{\theta_N^{n+1}-\theta_{N-1}^{n+1}}{2h^2}$$
$$-\frac{c^*}{r_N^2}r^2_{N-\frac{1}{2}}\frac{\theta_N^n-\theta_{N-1}^n}{2h^2}+g_N^{n+\frac{1}{2}} \quad (39)$$

Thus, a high-order compact finite difference scheme consists of (29) for interior grid points r_j, $j=2,\ldots N-1$ and (38)–(39) for two grid points r_1 and r_N. The truncation error at interior grid points $(r_j, t_{n+(1/2)})$, $j=2,\ldots,N$, of the scheme is of order $(\Delta t+h^4)$ and $(\Delta t+h^3)$ at grid points r_1 and r_N. Thus, from (29), (38), and (39), we get dimensionless temperature (θ).

4 Stability of Numerical Scheme

In this section, we show that the above-obtained schemes are unconditionally stable. Because of the limit on the text length, we will consider only the Case I. The stability of schemes obtained in Cases II and III can be showed by using the similar argument.

To discuss the stability of the numerical scheme obtained in *Case I*, we first rewrite the (12), (16), and (17) with no internal heat source, in vector matrix form as follows:

$$A\theta^1=B\theta^0,\quad n=0 \quad (40)$$

$$A\theta^{n+1}=B\theta^n+C\theta^{n-1},\quad n\geq1 \quad (41)$$

where $\theta^{n+1}=[\theta_1^{n+1},\theta_2^{n+1},\ldots..\theta_{N-1}^{n+1},\theta_N^{n+1}]^t$, and A, B, and C are the matrices involved in the above (41).

Now (41) can be written in equivalently as [25, 26]

$$U^{n+1}=DU^n \quad (42)$$

where

$$U^{n+1}=\begin{pmatrix}\theta^{n+1}\\ \theta^n\end{pmatrix},\ D=\begin{pmatrix}A^{-1}B & A^{-1}C\\ I & 0\end{pmatrix}_{N\times N} \quad (43)$$

This technique has reduced a three-level difference equation in time to a two level. Equation (42) will be stable when each eigenvalue of D has modulus ≤1, i.e. $\rho(D)\leq1$. From a computational point of view, the eigenvalues of D can be evaluated numerically. It is shown that the eigenvalues satisfy the stability condition. Our experience for solved examples shows that spectral radius of the corresponding D matrix stays <1, for various Δt and Δh.

In Figures 1–2, the eigenvalues of the D matrix are sketched. We show numerically that the upper bound for the absolute value of D's eigenvalues is <1 for all temporal grid size (Fig. 1) and spatial grid size (Fig. 2).

Tables 1–2 show the modulus of eigenvalues and corresponding eigenvectors for $N=8$ and 10, respectively. Thus, from the Figures 1 and 2 and Tables 1 and 2, it is clearly justify that $\rho(D)\leq1$ and hence scheme is unconditionally stable.

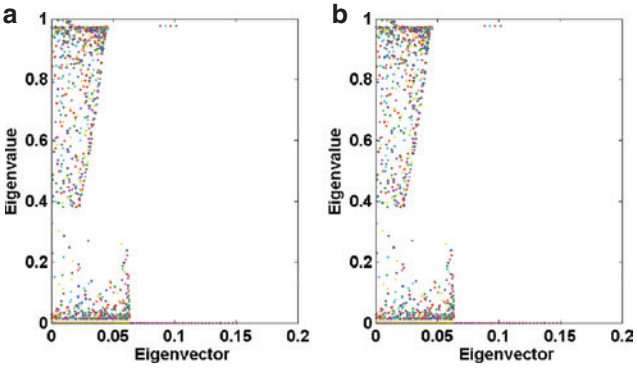

Figure 1: Variation of eigenvector with eigenvalue for $N=1000$ at (a) $\Delta t=0.01$; (b) $\Delta t=0.001$.

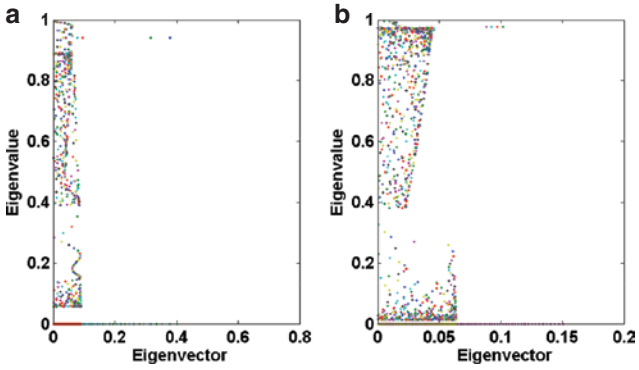

Figure 2: Variation of eigenvector with eigenvalue at $\Delta t = 0.001$ for (a) $N = 250$; (b) $N = 500$.

Table 1: For $N = 8$, modulus of eigenvalue and corresponding eigenvectors (of order 10^{-4}).

Eigenvalue	3562	3475	4651	2976	5826	2634	6283	5331
Eigenvector	9907	9907	9622	9073	5206	1947	164	320

5 Model Validation

To demonstrate the heat transport characteristics at small time and spatial scales, we consider the nondimensional form of the SPL heat conduction (7) for the thin film of silicon (*Si*). From hyperbolic two-step model [27–29], the physical constants of silicon film (*Si*) are as follows: thermal diffusivity $(\alpha) = 9.0 \times 10^{-7}$ m/s^2, thermal conductivity $(k) = 1$ W/mK, and phase lag of the heat flux vector $(\tau) = 5.0 \times 10^{-12}$ s. A simplification to the two-step model was proposed by [30] for the case of thin films exposed to picosecond. It was suggested that, for the silicon film, diffusion becomes negligible as the ratio of electron–phonon coupling to the electron thermal conductivity is much larger than one [31].

Figures 3 and 4 show the spatial temperature profile subjected to symmetric heating for very small thickness, i.e. 0.25 and 0.50 μm of film, respectively. This film thickness is smaller than the phonons mean free path, and hence, partial ballistic heat transport is expected [4]. For small heating period ($t \le 10^{-2}$), temperature of the thin film is suddenly jump at the boundaries, i.e. $x = 0.25$ and $x = 0.5$ as shown in Figures 3 and 4, respectively.

Figures 5 and 6 show the temperature profile in silicon film of thickness 1 and 2 μm, respectively, at various time periods. In this case, the hyperbolic heat transport phenomena dominates the ballistic heat transport. As expected from the SPL model, Figure 5 shows that the hyperbolic behavior for all heating period whatever be of macro or microscale order. From Figure 6, it is observed that, if the thickness of silicon film (L) >1 μm and t is very small (whatever macro or microscale order) then the wavy feature dominates the diffusive behavior, similar to the results found in [31].

From the above observations, it is clearly says that the SPL model gives the satisfactory results in the macro- and microtemporal scales and up to microspatial scales.

6 Numerical Examples

This section presents the complete investigation of accuracy and computational complexity by taking a particular example as follows

6.1 Accuracy of Numerical Scheme

To verify the accuracy of our numerical scheme, we first consider a simple example

$$2\frac{\partial\theta}{\partial t} + \frac{\partial^2\theta}{\partial t^2} = \frac{\partial^2\theta}{\partial x^2} + \left(g + \frac{1}{2}\frac{\partial g}{\partial t}\right) \tag{44}$$

$$\theta(x, 0) = \cos x, \quad \frac{\partial\theta(x, 0)}{\partial t} = 0 \tag{45}$$

$$\frac{\partial\theta(0, t)}{\partial x} = 0, \quad \frac{\partial\theta(l, t)}{\partial x} = 0 \tag{46}$$

where the exact solution is $\theta(x, t) = (1+t)e^{-t}\cos x$. We employed the high-order Crank–Nicholson finite difference scheme to solve the above problem.

Since the analytical solution becomes very small for large t, the maximum l_2-norm errors of the numerical solutions as compared with the analytical solution was computed for $0 \le t \le 1$ based on the formula

Table 2: For $N = 10$, modulus of eigenvalue and corresponding eigenvectors (of order 10^{-4}).

Eigenvalue	3209	3116	4286	4352	1091	5647	3389	6187	5068	4224
Eigenvector	9906	9906	8506	9403	9666	3910	3910	522	153	232

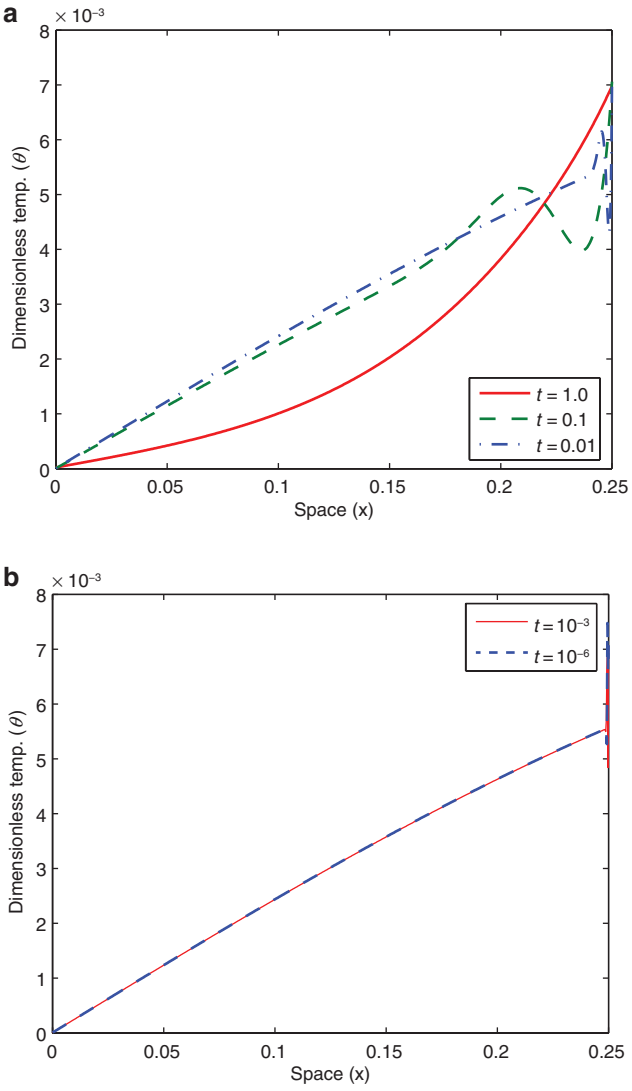

Figure 3: Spatial temperature profile for silicon film of thickness $(L) = 0.25$ μm.

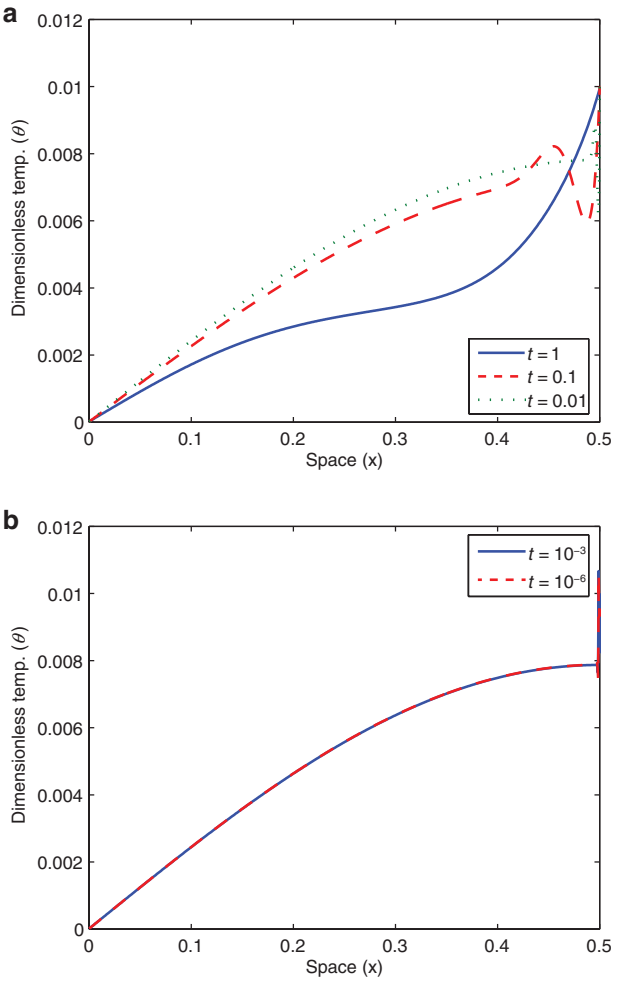

Figure 4: Spatial temperature profile for silicon film of thickness $(L) = 0.5$ μm.

$$E(N, \Delta t) = \max_{0 \le n\Delta t \le 1} \sqrt{h \sum_{j=1}^{N} [\theta_j^n - \theta^{exact}(x_j, t_n)]^2} \qquad (47)$$

To obtain the convergence rate with respect to the spatial variable, Dai [21] assume that $E(N, \Delta t) = O(\Delta^p + h^q)$. If Δt is small enough, then $E(N, \Delta t) \approx O(h^q)$. Consequently, $\frac{E(N, \Delta t)}{E(2N, \Delta t)} \approx 2^q$ and hence $q \approx \log_2 \left[\frac{E(N, \Delta t)}{E(2N, \Delta t)} \right]$ is the convergence rate with respect to the spatial variable. Similarly, $p \approx \log_2 \left[\frac{E(N, 2\Delta t)}{E(N, \Delta t)} \right]$ is the convergence rate with respect to the temporal variable.

The maximal l_2-norm errors together with the temporal and spatial convergence rate of the numerical scheme

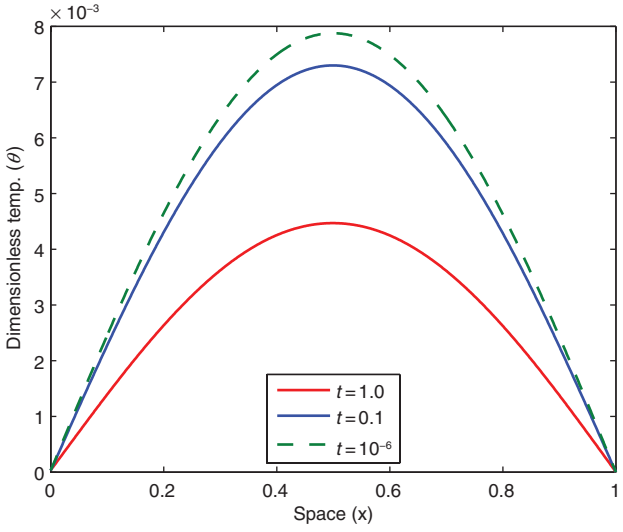

Figure 5: Spatial temperature profile for silicon film of thickness $(L) = 1.0$ μm.

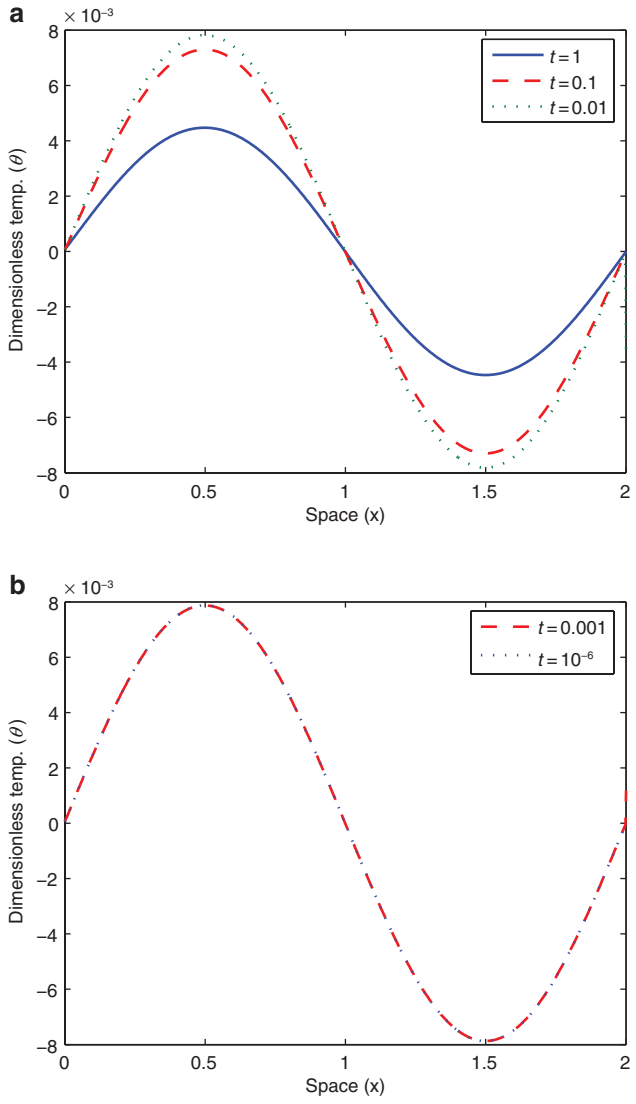

Figure 6: Spatial temperature profile for silicon film of thickness $(L) = 2.0\ \mu m$.

Table 3: Maximum l_2-norm errors $E(N, \Delta t)$ and convergence rate for $N = 10{,}001$ and $0 \le t \le 1$.

Δt	$E(N, \Delta t)$	Temporal convergence rate
0.01	1.7321×10^{-4}	–
0.001	3.6725×10^{-5}	2.117
0.0005	6.4158×10^{-5}	2.064
0.0001	1.5377×10^{-5}	2.000

are given in Tables 3 and 4, respectively. A close examination of Tables 3 and 4 show that errors of the scheme minimises on decreasing the spatial and temporal grid size. The temporal and spatial convergence rate are almost >2 (Tables 3 and 4).

Table 4: Maximum l_2-norm errors $E(N, \Delta t)$ and convergence rate for $\Delta t = 10^{-6}$ and $0 \le t \le 1$.

Grids	$E(N, \Delta t)$	Spatial convergence rate
51	9.9872×10^{-4}	–
101	5.6650×10^{-5}	2.009
201	5.0485×10^{-5}	2.012
501	6.5133×10^{-6}	2.003

6.2 Computational Complexity

According to (40)–(41), to calculate the value of θ^n, $(n > 0)$, where n is the number of iteration, we need to initiate a loop that will iterate n times (from loop index 1 to n) and at each step it will calculate the value of θ^j (where j is the loop index), which is actually $O(N^{2.807})$ operations, where $N \times N$ is the order of matrices A, B, and C. So the time complexity of the proposed method is $O(n * N^{2.807})$. More about complexity is given in [32, 33].

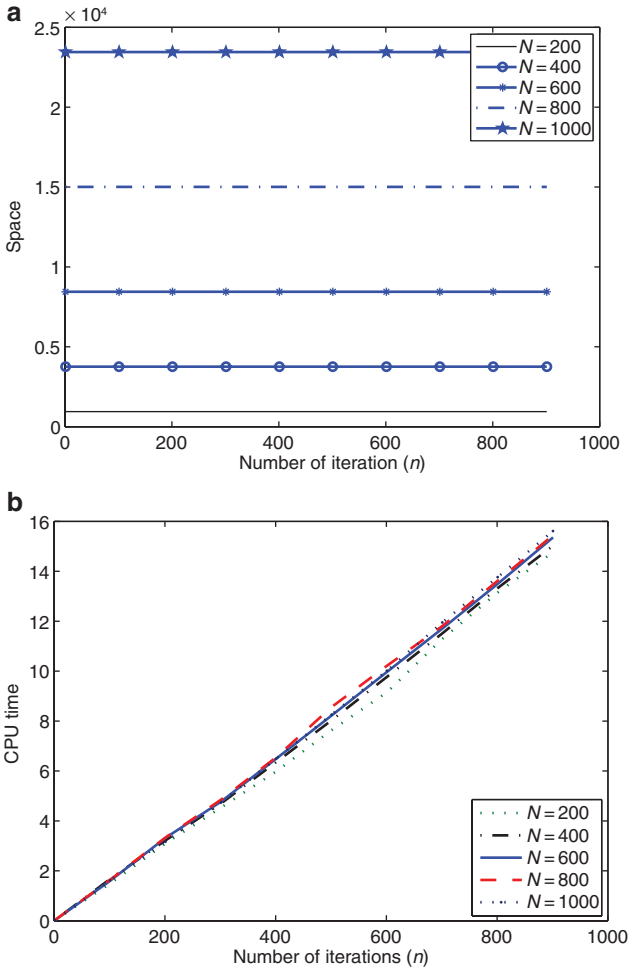

Figure 7: Variation of number of iterations (n) with (a) space; (b) time.

Variation of n with time and space is given in Figure 7. Figure 7(b) represents time required to calculate θ^n with respect to n for different values of N. For any fixed value of N, time complexity of the proposed method is linear with respect to n.

To calculate the value of θ^j at each iteration step, we need to store only the matrices A, B, C, and θ^{j-1}. So space complexity of the proposed method is of $O(N^2)$. Figure 7(a) represents requirement of space to calculate θ^n with respect to n, for different values of N. It is to be noted that for any fixed value of N, space requirement is constant with respect to n. So for any fixed N, calculation of θ^j and $\theta^{j\pm1}$ will need same amount of space. This is the main advantage of this scheme.

7 Conclusion

A mathematical model of the SPL heat conduction for general body heated by laser heat source is solved by high-order finite difference scheme, which avoids the need of discretising Neumann boundary condition. The effects of spatial and temporal grid size on the stability of the scheme have investigated and found that the scheme is independent of grid size and hence unconditionally stable. Validation of the SPL model has investigated by taking thin film of silicon and observed that present model is applicable for very small temporal size of microscale order and up to microspatial size.

Nomenclature

A	a matrix of order $N\times N$
B	a matrix of order $N\times N$
C	a matrix of order $N\times N$
c	thermal wave propagation speed, m/s
c_b	specific heat capacity, J/kgK
f_r	reference heat flux
g^*	internal heat source, W/m^3
g	dimensionless internal heat source, $\frac{4\alpha g^\star}{cf_r}$
k	thermal conductivity, W/mK
l	dimensionless length of heat conduction medium
q^*	heat flux, W/m^2
q	dimensionless heat flux, $\frac{q^*}{f_r}$
r	position vector
t^*	time, s
t	dimensionless time, $\frac{c^2t^*}{2\alpha}$
Δt	temporal grid size
T	temperature, K
∇T	temperature gradient, K/m
x	dimensionless spatial coordinate, $\frac{cy}{2\alpha}$
Δx	spatial grid size (=h)
y	spatial coordinate, m
α	thermal diffusivity, m^2/s
θ	dimensionless temperature, $\frac{kcT}{\alpha f_r}$
ρ	density, kg/m^3
τ	lagging time, s

Acknowledgments: The authors of this article express their sincere thanks to the respected reviewers and editors for their valuable suggestions in the improvement of the article. The authors are also thankful to the DST-CIMS, BHU, for providing the necessary facilities during the manuscript.

References

[1] C. Cattaneo, C. R. Acad. Sci. **247**, 431 (1958).
[2] M. P. Vernotte, J. Comput. Phys. **246**, 3154 (1958).
[3] D. G. Cahill, W. K. Ford, K. E. Goodson, G. D. Mahan, A. Majumdar, et al., J. Appl. Phys. **93**, 793 (2003).
[4] A. A. Joshi and A. Majumdar, J. Appl. Phys. **74**, 31 (1993).
[5] C. L. Tien, A. Majumdar, and F. M. Gerner, Microscale Energy Transport, Taylor & Francis, Washington 1998.
[6] L. Q. Wang, X. Zhou, and X. Wei, Heat Conduction: Mathematical Models and Analytical Solutions, Springer-Verlag, Berlin 2008.
[7] D. D. Joseph and L. Preziosi, Rev. Modern Phys. **61**, 41 (1989).
[8] M. N. Ozisik and D. Y. Tzou, ASME J. Heat Trans. **116**, 526 (1994).
[9] D. Y. Tzou, ASME J. Heat Trans. **111**, 232 (1989).
[10] D. Y. Tzou, Int. J. Heat Mass Trans. **32**, 1979 (1989).
[11] D. Y. Tzou, ASME J. Heat Trans. **112**, 21 (1990).
[12] D. Y. Tzou, Int. J. Heat Mass Trans. **35**, 877 (1990).
[13] D. Y. Tzou, Annu. Rev. Heat Trans. **4**, 111 (1992).
[14] D. Y. Tzou and W. Dai, Int. J. Heat Mass Trans. **52**, 1206 (2009).
[15] A. Faghri and Y. Zhang, Transport Phenomena in Multiphase Systems, Elsvier, UK 2006.
[16] A. W. Abu-Qare and M. B. Abou-Donia, Food Chem. Toxicol. **40**, 1327 (2002).
[17] W. Liao, J. Zhu and A. Q. M. Khaliq, Numer. Meth. Part. Differ. Equ. **22**, 600 (2005).
[18] B. L. Wang and J. C. Han, Int. J. Eng. Sci. **55**, 66 (2012).
[19] K. W. Morton and D. F. Mayers, Numerical Solution of Partial Differential Equations, Cambridge University Press, New York 2005.
[20] J. W. Thomas, Numerical Partial Differential Equations: Finite Difference Methods, Springer-Verlag, New York 1995.
[21] W. Dai, Int. J. Ther. Sci. **49**, 571 (2010).
[22] S. K. Lele, J. Comput. Phys. **103**, 16 (1992).
[23] J. Zhao, W. Dai, and S. Zhang, Numer. Meth. Part. Differ. Equat. **24**, 165 (2008).
[24] T. N. Mishra, S. Sarkar, and K. N. Rai, J. Appl. Math. Comput. **236**, 693 (2014).

[25] A. Malek and S. H. Momeni-Masuleh, J. Comput. Appl. Math. **217**, 137 (2008).
[26] A. Malek, Z. K. Bojdi, and P. N. Golbarg, ASME J. Heat Trans. **134**, 41 (2012).
[27] T. Q. Que and C. L. Tien, Int. J. Heat Mass Trans. **35**, 719 (1992).
[28] T. Q. Que and C. L. Tien, J. Heat Trans. **115**, 835 (1993).
[29] D. Y. Tzou, ASME J. Heat Trans. **117**, 8 (1995).
[30] M. A. Al-Nimr and V. S. Arpaci, Int. J Heat Mass Trans. **43**, 2021 (2001).
[31] R. Nassr and W. Dai, Modelling of Microfabrication Systems, Springer-Verlag, Berlin 2003.
[32] H. C. Thomas, E. L. Charles, L. R. Ronald, and C. Stein, Introduction to Algorithms, MIT Press, Cambridge 2002.
[33] C. K. Dexter, The Design and Analysis of Algorithms, Springer-Verlag, New York 1992.